THE EUROPEAN
PHYSICAL JOURNAL D

Atom interferometry gravity-gradiometer for the determination of the Newtonian gravitational constant G

A. Bertoldi, G. Lamporesi, L. Cacciapuoti[a], M. de Angelis[b], M. Fattori[c], T. Petelski[d], A. Peters[e], M. Prevedelli[f], J. Stuhler[c], and G.M. Tino[g]

Dipartimento di Fisica and LENS, Università di Firenze, INFN, Sezione di Firenze, Via Sansone 1,
50019 Sesto Fiorentino (Firenze), Italy

Abstract. We developed a gravity-gradiometer based on atom interferometry for the determination of the Newtonian gravitational constant G. The apparatus, combining a Rb fountain, Raman interferometry and a juggling scheme for fast launch of two atomic clouds, was specifically designed to reduce possible systematic effects. We present instrument performances and preliminary results for the measurement of G with a relative uncertainty of 1%. A discussion of projected accuracy for G measurement using this new scheme shows that the results of the experiment will be significant to discriminate between previous inconsistent values.

PACS. 03.75.Dg Atom and neutron interferometry – 04.80.-y Experimental studies of gravity – 06.20.Jr Determination of fundamental constants

Highlight Paper

1 Introduction

Recent advances in atom interferometry led to the development of new methods for fundamental physics experiments and for applications [1,2]. In particular, atom interferometers are new tools for experimental gravitation as, for example, for precision measurements of gravity acceleration [3], gravity gradients [4], equivalence principle tests [5], $1/r^2$ law test [6–8], and for possible applications in geophysics [3,9]. Ongoing studies show that future experiments in space [6] will allow to take full advantage of the potential sensitivity of atom interferometers using, for example, atom gyroscopes [10,11] to test general relativity predictions [12]. The possibility of using atom interferometry for gravitational waves detection was also investigated [13–15].

In this paper, we describe an atom interferometer developed for a precise determination of the Newtonian gravitational constant G. The basic idea of the experiment and the planned precision were presented in [16]. Here we discuss the interferometer performances and show that the sensor is able to detect the gravitational field induced by source masses. The projected accuracy for G measurement using this new scheme shows that the results of the experiment will be significant to discriminate between existing inconsistent values.

In fact, because of the importance of this fundamental physical constant, more than 300 experiments were performed to determine its value but the results are not in agreement. As a result, the present recommended CODATA value ($G = 6.6742(10) \times 10^{-11}$ m^{3}kg^{-1}s^{-2}) is affected by an uncertainty of 150 ppm, which is much larger than for any other fundamental physical constant [17]. With a few exceptions, most experiments were performed using conceptually similar schemes based on suspended macroscopic masses as probes and torsion balances or pendula as detectors.

In our experiment, freely falling atoms act as probes of the gravitational field and an atom interferometry scheme is used to measure the effect of nearby well-characterized source masses (Fig. 1). ^{87}Rb atoms, trapped and cooled in a magneto–optical trap (MOT), are launched upwards in a vertical vacuum tube with a moving optical molasses scheme, producing an atomic fountain. Near the apogee of the atomic trajectory, a measurement of their

[a] European Space Agency, ESTEC, 2200 AG Nordwijk, NL.

[b] *On leave from*: Istituto Cibernetica CNR, 80078 Pozzuoli, Italy.

[c] *Present address*: 5. Physikalisches Institut, Universität Stuttgart, 70550 Stuttgart, Germany.

[d] *Present address*: European Patent Office, 80469 München, Germany.

[e] Institut für Physik, Humboldt–Universität zu Berlin, 10117 Berlin, Germany.

[f] Dipartimento di Chimica Fisica e Inorganica, Università di Bologna, 40136 Bologna, Italy.

[g] e-mail: `guglielmo.tino@fi.infn.it`
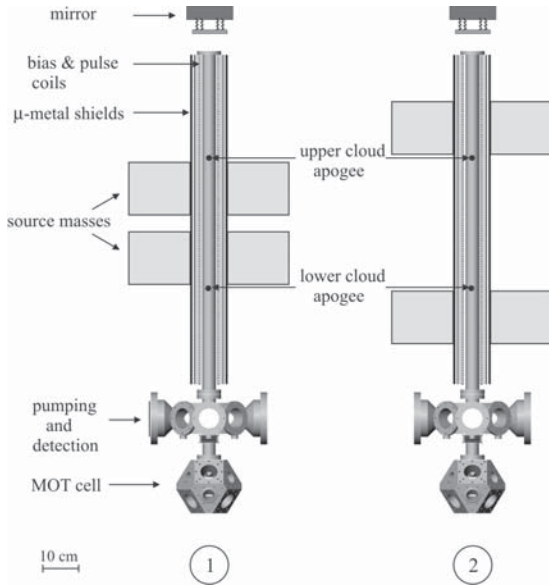
Fig. 1. Scheme of the experimental apparatus showing the atomic fountain set-up and the two source masses configurations. The laser beams and optical system are not shown.

vertical acceleration is performed by a Raman interferometry scheme [18]. External source masses are positioned in two different configurations and the induced phase shift is measured as a function of masses positions. In order to suppress common-mode noise and to reduce systematic effects, a double-differential scheme has been adopted. The vertical acceleration is simultaneously measured in two vertically separated positions with two atomic samples, that are launched in rapid sequence with a juggling method. From the differential acceleration measurements as a function of the position of source masses, and from the knowledge of the mass distribution, the value of G can be determined.

The paper is organized as follows: in Section 2 we introduce Raman interferometry and the basic idea of the experiment to measure G. Section 3 describes the apparatus and the experimental sequence. A characterization of interferometer and gradiometer performances is presented in Section 4. In Section 5 we report on the detection of external source masses and a preliminary measurement of G. The expected performance with the final configuration and the projected accuracy in the measurement of G are also discussed.

2 Raman interferometry basics and idea of the experiment

In this section, we discuss the basic idea of the experiment, the scheme of Raman interferometry and its application to measure G. A more detailed discussion can be found in [16] and references therein.

In a Raman interferometry-based gravimeter, atoms in an atomic fountain are illuminated by a sequence of three light pulses. The light pulses are realized with two

laser beams, which have frequencies ω_1 and ω_2 close to transitions of a Λ-type three-level atom with two lower states $|a\rangle$ and $|b\rangle$ and an excited state $|e\rangle$. The laser beams propagate along the vertical z-axis in opposite directions and with wavevectors $\mathbf{k}_1 = k_1\,\mathbf{e}_z$ and $\mathbf{k}_2 = -k_2\,\mathbf{e}_z$ ($k_i = \omega_i/c$, $i = 1, 2$). The light pulses drive two-photon Raman transitions between $|a\rangle$ and $|b\rangle$. A π-pulse, which has a duration of $\tau = \pi/\Omega$ (Ω being the two photon Rabi frequency), switches the atomic state from $|a\rangle$ to $|b\rangle$ or vice versa. A $\pi/2$-pulse with duration $\tau = \pi/(2\Omega)$ splits the atom wavefunction into an equal superposition of $|a\rangle$ and $|b\rangle$. Besides altering the real amplitudes α, β of the atomic wavefunction $\Psi = \alpha\,e^{i\Phi_\alpha}|a\rangle + \beta\,e^{i\Phi_\beta}|b\rangle$, the light field can also modify the atomic momentum and the phase. An atom that changes its internal state changes its momentum by an amount of $\hbar\,k_{\mathrm{eff}} = \hbar\,(k_1 + k_2)$. At the same time, the phases $\Phi_{\alpha,\beta}$ are modified according to the local phase of the light field.

The interferometer is composed of a $\pi/2$-π-$\pi/2$ pulse sequence. The three pulses, each separated by the time T, produce (in space-time) the two interfering paths, I and II. The first $\pi/2$ pulse splits the atomic wave packet, the π pulse induces the internal and external state inversion, the last $\pi/2$ pulse finally recombines the matter waves after their different space–time evolution. After recombination of the two paths, at the output of the interferometer the probability of finding the atoms in state $|a\rangle$ shows a typical interference-like behaviour:

$$N_a/N \propto 1 - \cos(\Phi_{\mathrm{I}} - \Phi_{\mathrm{II}}) \tag{1}$$

where $\Phi_{\mathrm{I,II}}$ are the phases accumulated on path I and II, respectively. The phases Φ_{I} and Φ_{II} depend on the local phase of the light field as seen by the atoms during Raman pulses. This links the vertical atomic position to the phase evolution of the laser field. The phase evolution depends on the effective frequency $\omega_{\mathrm{eff}}(t) = \omega_1(t) - \omega_2(t)$ and on the phase relation between the Raman pulses. Usually, one varies the effective frequency linearly in time to compensate for the first order Doppler effect of the free-falling atoms and keep the Raman resonance condition (effective frequency matching the energy splitting of the two lower states). With $\omega_{\mathrm{eff}}(t) = \omega_{\mathrm{eff},0} - \beta t$ one then obtains:

$$\Phi_{\mathrm{I}} - \Phi_{\mathrm{II}} = (\beta - k_{\mathrm{eff}}g)T^2 - \phi(0) + 2\phi(T) - \phi(2T). \tag{2}$$

The compensation of the Doppler effect ($\beta = k_{\mathrm{eff}}g$) and an unperturbed evolution of the laser phase ϕ leads to $\Phi_{\mathrm{I}} - \Phi_{\mathrm{II}} = 0$. Actively changing the laser phase between T and $2T$ by $\delta\phi$ will result in $\phi(2T) = \phi(0) + \delta\phi = \phi(T) + \delta\phi$ and hence $\Phi_{\mathrm{I}} - \Phi_{\mathrm{II}} = -\delta\phi$. In this way, one can scan the interference fringe to prove $(\beta - k_{\mathrm{eff}}g) = 0$ (for right β) or reveal the phase offset $(\beta - k_{\mathrm{eff}}g)T^2$ (for imperfect Doppler compensation). In both cases, the value of g is obtained combining the measured phase offset and the value of β, which is set by a frequency generator.

For the measurement of G, we use a Raman interferometer to detect the change in atoms acceleration induced by external source masses. In order to achieve high sensitivity and accuracy, however, the experimental scheme was developed with important specific features.

First, we launch two clouds of atoms to realize two fountains that are displaced vertically (see Fig. 1). The Raman pulses act on both clouds simultaneously and generate two interferometers at the same time. In the detection of the differential phase shift between the two interferometers, spatially homogeneous accelerations cancel out and common mode measurement noise is reduced. The two-clouds set-up results in an atomic gravity gradiometer. If the trajectory of the first cloud is located above the source masses, atoms will experience an induced acceleration in $-z$-direction. In contrast, choosing the trajectory of the second cloud below the source masses, the induced acceleration of this cloud will be in $+z$-direction. Taking the difference of these two accelerations yields a signal, which is about twice the one obtained with only one cloud.

Second, we determine the differential interferometer phase shifts with the source masses at distinct positions (positions 1 and 2 in Fig. 1). Evaluating the difference between the measurements further reduces systematic spurious effects if they are constant over the time scale of the source masses repositioning.

Third, the atomic trajectories and the shape and positioning of source masses can be optimized to reduce experimental sensitivity to crucial parameters like precision and stability of the atomic fountain. As discussed in detail in Section 5, the two interferometers will be performed in regions where the measured phase is stationary with respect to the clouds position in both masses configurations.

The combination of these features will allow to reach the targeted accuracy $\Delta G/G \approx 10^{-4}$.

3 Experimental set-up

The experimental apparatus consists of the vacuum chamber, the laser sources and optical set-up for the production of the double fountain of Rb atoms using a juggling procedure, the apparatus for Raman pulse interferometry, and the system of source masses, their support and precision positioning components. The experimental sequence, timing and data acquisition are computer controlled. In this section, we describe the main parts of the apparatus. More details can be found in [19].

3.1 Atomic fountain and juggling apparatus

The fountain of ^{87}Rb atoms is produced using a magneto-optical trap and moving–molasses scheme. The laser beams are in a 1-1-1 six-beam σ^+/σ^- configuration. This keeps the central vertical axis free for the Raman laser beams and allows to realize a stable and precise atomic fountain.

The relevant parts of the vacuum system are shown in Figure 1. It consists of three main parts: the lowest part is a titanium cube with cut edges where atoms are trapped in the MOT from the vapour produced by a dispenser (SAES Getters 5G0807), cooled and launched in the fountain. The middle part of the vacuum system is a thermally demagnetized 316 LN stainless steel cell. This cell is used

for pumping and to detect the atoms. The top part of the vacuum system is the interferometer tube. It is 1 m long, has a diameter of 40 mm and is made of titanium. The tube is magnetically shielded with two coaxial cylinders of μ–metal (Amuneal) that are 0.76 mm thick and 1 m long, with internal diameters of 74 mm and 84 mm. The attenuation of the radial and axial components of the external field is 76 dB and 69 dB, respectively. The saturation field B_S is about 6 mT.

A magnetic field gradient of 75 mT/m in the MOT region is generated by a water-cooled pair of coils in anti–Helmholtz configuration. The cooling radiation is generated by a tapered amplifier delivering 500 mW output power. It is injected with 25 mW from a laser (New Focus Vortex 6000, 65 mW at 125 mA) frequency–stabilized on the $5\,^2S_{1/2}$, $F = 2 \rightarrow 5^2P_{3/2}$, $F = 3$ transition of ^{87}Rb. This laser also acts as the main frequency reference for the experiment. The radiation for the MOT is detuned by 3Γ ($\Gamma = 2\pi \times 6.1$ MHz) to the red of the resonance.

Repumping light is provided by an extended cavity diode laser, frequency–locked to the reference laser and optically injecting a slave diode laser.

Cooling light is coupled into fibers that are connected to an integrated fiber splitter system (Schäfter&Kirchhof) which distributes the light to the six MOT beams which have an intensity of 4.2 mW/cm^2 each with 11 mm beam waist. Each beam is delivered to the MOT region through a collimator rigidly fixed to the cell. Hyperfine repumping light is provided by a beam in one direction with an intensity of 0.8 mW/cm^2.

Under standard operating conditions, $\sim10^9$ atoms are loaded in the MOT with a typical loading time $\tau = 2.5$ s. The MOT has a size of ~4 mm.

The atomic cloud is launched into the fountain tube by using the moving molasses method. The laser beams propagating upwards and downwards are separately controlled by two acousto–optic modulators (AOMs). By applying a detuning $\delta\omega$ of opposite sign to the upper and lower beams, the atoms are forced to move along the vertical direction with a velocity

$$v = \frac{\delta\omega}{k\,\cos\xi} \qquad (3)$$

where k is the wave vector of the cooling radiation and ξ the common angle between each of the six beams and the vertical direction ($\cos\xi = 1/\sqrt{3}$). During the launch, the detuning of the cooling beams in the moving frame is increased and their intensity is reduced. This sequence allows to further cool the atomic sample in the moving molasses frame. The launch sequence for one cloud is realized in four steps (Fig. 2). After the MOT magnetic field is switched off, the atoms are launched upwards by introducing a detuning of opposite sign to the three upwards- and downwards-propagating laser beams. After 2.5 ms, the intensity of each beams is lowered to the saturation intensity $I_s = 1.7$ mW/cm^2 and the mean detuning is increased to $-6.3\,\Gamma$. After 1.8 ms, the intensity of the cooling beams is reduced by a factor of 3.5 for 0.3 ms. Finally, the cooling beams are switched off, leaving only the repumper
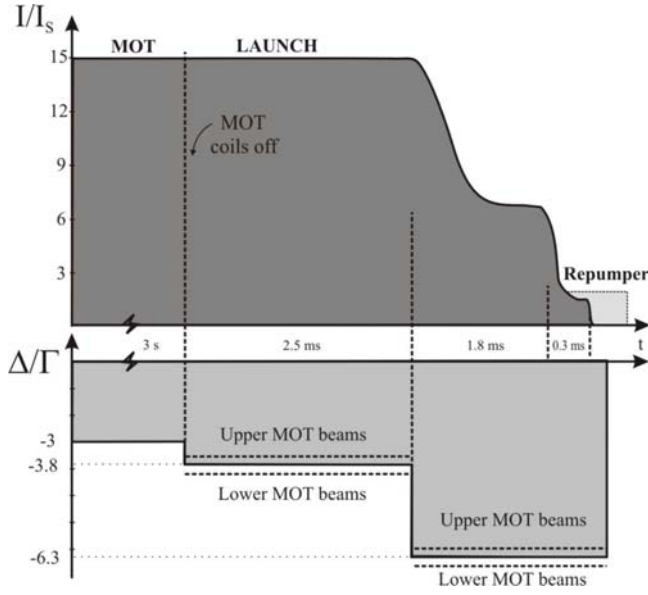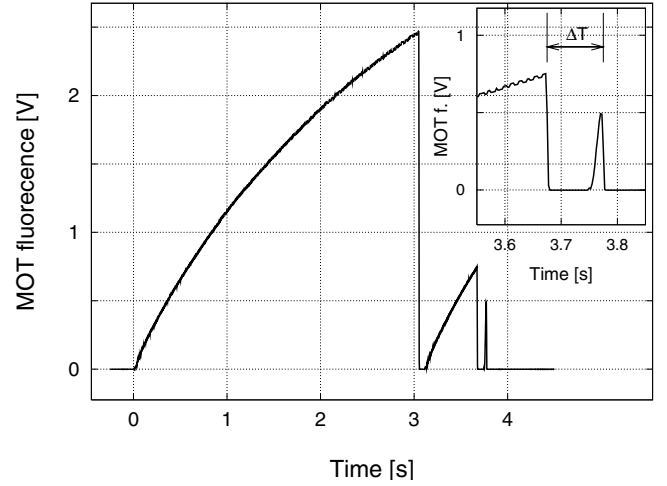
Fig. 2. Sequence used in the experiment to launch cold atoms in the fountain. Horizontal dashed lines represent the different frequencies for the downwards- and upwards-propagating beams. The time axis is not to scale.

Fig. 3. MOT Fluorescence detected during a juggling sequence. The first two clouds are slowly loaded from background gas. The third one is obtained trapping the first cloud falling down in the MOT region. The inset shows the launch of the last two clouds in a time interval of 100 ms.

beam on to optically pump the atoms into the $F = 2$ state with a measured efficiency of more than 99.9%.

The temperature of the sample, measured by monitoring its axial expansion during free fall, is approximately 4 μK. The number fluctuation from launch to launch is about 3%. The fountain sequence was synchronized to the 50 Hz power line in order to stabilize the whole system and to gain in reproducibility. The effect of this triggering can introduce a phase term in the single measurement, but it is cancelled out when considering the difference between signals corresponding to two different masses configurations. This can be checked by varying the trigger delay.

The gradiometer requires two clouds of cold atoms moving with the same velocity at the same time, but vertically displaced. The adopted vertical separation of 35 cm between the two clouds and apogees at 60 cm and 95 cm above the MOT requires a launch delay between the two samples of 90 ms. The two atomic clouds are prepared within such a short time using a juggling technique [20]. In our experimental sequence, a first atomic cloud is launched 60 cm high and is recaptured with an efficiency of 25%. The dominant loss process is the thermal expansion of the cloud. During the ballistic flight of the first cloud, a second one is loaded from the background vapour. 80 ms before the first cloud falls down in the MOT region, the second one is launched. The first cloud, used as a cold and intense source of atoms, is then recaptured, cooled and launched upwards within 25 ms (Fig. 3). Increasing the loading time of the first cloud results in a higher number of recaptured atoms, but the experimental repetition rate is reduced, and so the instrument sensitivity. The loading time for the first cloud was set in order to have an experimental sequence duration of about 5 s, as shown in Figure 3. The number of atoms launched in each of the two clouds used in the gradiometer is then 5×10^8.

3.2 State preparation procedure

After the launch, the atoms are selected both in velocity and by their m_F state. The selection procedure uses vertical beams so that the state preparation can take place simultaneously on both clouds. The selection is realized in the vacuum tube, where a uniform vertical bias field of 25 μT is applied. The sequence starts by blowing away the atoms remaining in the $F = 1$ state after the launch, by applying a pulse of elliptically polarized radiation resonant with the $F = 1 \rightarrow F' = 0$ transition. The measured efficiency for a 10 ms long pulse is about 50%, limited by the presence of dark states. A narrow selection of the vertical velocity distribution of atoms in the $F = 2$, $m_F = 0$ is transferred to the $F = 1$, $m_F = 0$ state using a 100 μs long velocity–selective Raman pulse. The atoms in the $F = 2$ state are removed from the sample by applying a circularly polarized vertical beam for 5 ms, resonant with the $F = 2 \rightarrow F' = 3$ transition.

After the selection sequence, the atoms end up in the $F = 1$, $m_F = 0$ state with a horizontal temperature of 4 μK and a vertical temperature of 40 nK, corresponding to velocity distribution widths (HWHM) respectively of 3.3 v_{rec} and 0.3 v_{rec} ($v_{rec} = 6$ mm/s for Rb resonance transition).

3.3 Raman interferometer apparatus

Stimulated Raman transitions are driven by light from two extended-cavity phase–locked diode lasers, with a relative frequency difference equal to the ^{87}Rb ground state hyperfine splitting frequency ($\nu_{hf} = 6.835$ GHz) and amplified

by a single tapered amplifier. The detuning from the D_2 resonance is -3.3 GHz.

The laser locking system was described in detail in [21]. The two main requirements of the optical phase–locked–loop (OPLL) are robustness, necessary for continuous operation over long periods of time, and low rms phase error $\sqrt{\langle\varphi^2\rangle}$. The latter is not a limiting parameter for the gradiometer, because of the phase noise rejection due to the differential measurement scheme. These requirements are accomplished using a detector that combines in a mutually exclusive way a digital phase and frequency detector and an analog phase detector. The digital detector has a capture range of the order of 100 MHz and it allows about 10 hours of continuous operation with the two lasers phase–locked. The analog detector ensures a low noise spectral density necessary for accurate phase–locking. The resulting noise of the interferometer phase Φ, taking into account the interferometer transfer function [24], is $\delta\Phi = 1$ mrad.

The master laser is an extended-cavity diode laser (New Focus Vortex 6000, 65 mW at 130 mA). The slave laser is an anti–reflection coated diode (Sacher SAL–0780–040, 35 mW at 60 mA) mounted in an extended cavity. The master and the slave beams are combined on a polarizing beam splitter followed by a linear polarizer. One output of the beam splitter is sent to a fast photodiode to generate the beat note. The second output injection–seeds a tapered amplifier, whose astigmatism is corrected for with a cylindrical lens. A hot Rb cell filters resonant light in the spectral wings of the amplifier output.

The pulse timing of the Raman beams during the interferometer sequence is controlled by an AOM, driven by a waveform generator (Agilent 33220A). After the AOM, the beams are coupled into a polarization–maintaining fiber, which acts as a spatial filter. The fiber output is collimated by an aspherical lens ($f = 1000$ mm) to obtain a beam waist of 10 mm. Most of the optical elements on the path of the Raman beams have a $(\lambda/20)$ quality to avoid phase–front distortions.

The Raman beams enter the vacuum system through the lower window of the MOT cell and exit through the window at the top of the interferometer tube. After passing through a quarter–wave plate, they are retroreflected by a mirror, thus obtaining a $lin\perp lin$ configuration in the interferometer region. The horizontality of the retroreflecting mirror has been adjusted within 20 μrad using a tiltmeter (Applied Geomechanics 755–1129). Taking into account the Doppler effect and considering the polarization of the beams, only Raman transitions with $\Delta m_F = 0$ are possible for atoms with non zero velocity. To compensate for the varying Doppler shift of the atomic resonance during the atoms free–fall trajectory, the Raman beams frequency difference is linearly swept using a continuous–phase waveform generator (Agilent 33250A). The central π pulse of the interferometer sequence is sent 5 ms before the atoms reach the top of their trajectory, when their velocity is still high enough to discriminate between upwards and downwards propagating Raman beams. For

a Raman beam intensity of 30 mW/cm^2, the π pulse lasts 100 μs.

The interferometric phase shifts are detected using the relative phase of the Raman beams as a reference. To scan the interferometric fringes, a controlled phase jump ϕ_{L} is applied after the π pulse to the rf signal generated by the low–phase–noise reference oscillator (Anritsu MG3692A).
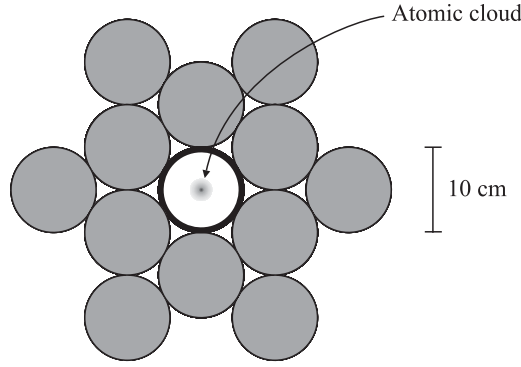
Coils wound between the vacuum tube and the magnetic shield enable a precise control of the magnetic field during the interferometer sequence. A solenoid, of 1 m length, generates a vertical bias magnetic field on the z-axis, chosen as quantization direction in the interferometric region. A series of 10 coils, each 9 cm long, are used to add a controlled phase shift via the second–order Zeeman shift on the atoms during the interferometer sequence.

3.4 Detection scheme

After the interferometric sequence, the population of the two hyperfine sublevels of the ground state is measured in the intermediate chamber using normalized fluorescence detection. The falling clouds pass through two horizontal counterpropagating circularly–polarized beams, with a vertical distance of 20 mm. The typical time interval of about 100 ms between the detection of the two vertically separated clouds prevents cross talk signals for the two interferometers. The beams have a rectangular section of (13×6) mm^2, and their wave vector $\mathbf{k}$ is parallel to a local magnetic field. Each beam has a power of 1 mW and is resonant with the $F = 2 \leftrightarrow F' = 3$ transition, in order to interact with atoms in the $F = 2$ state. The lower part of the higher beam is not retroreflected in order to horizontally blow–away the atoms after detection. On the lower probe beam 0.4 mW of repumping light is overlapped to optically pump atoms from the $F = 1$ state to the closed $F = 2 \leftrightarrow F' = 3$ transition. With this configuration, atoms in the $F = 2$ state are detected with the higher beam and atoms in the $F = 1$ state with the lower one. The fluorescence photons from the two detection regions are collected by a 5 cm diameter lens ($f = 100$ mm) placed at a distance of 130 mm and separately focused onto two large area photodiodes (Hamamatsu S7539). The population fractions in the two states are obtained via normalization, eliminating the shot–to–shot dependence on atom number. With a typical number of 5×10^4 detected atoms per cloud in each state, the signal-to-noise ratio is 60/1, limited by background light.

3.5 Source masses set-up

Two sets of masses are used to generate a well-known gravitational field. Each set is made of 12 identical cylinders, symmetrically arranged in a hexagonal configuration around the vertical axis of the atomic fountain (Fig. 4). The cylinders have a diameter of 100 mm and a height of 150 mm. The two sets of masses are held by two titanium rings, which are connected to a precision translation

Highlight Paper

Fig. 4. Source masses position around the interferometer tube (top view).

Fig. 5. Fringes recorded with a single atom interferometer for $T = 20$ ms delay between Raman pulses. The active vibration isolation system of the mirror was off during the first five cycles (empty squares) and on during the last five (filled squares). The acquisition time for each data set (5 cycles) was 900 s. The solid lines are sinusoidal least–square fits over the two sets of data. The phase uncertainty is 33 mrad in the first case and 10 mrad in the second case.

stage specifically designed for the experiment. This allows to move vertically the two sets of masses and to position them at a relative distance ranging between 4 and 50 cm. The distance is measured with two linear optical encoders (Heidenhain LS603). A test of the system with a laser–tracker showed a reproducibility of ± 1 μm.

In the final configuration for the G measurement, well-characterized W masses will be used (see Sect. 5). The results reported in this paper were instead obtained using Pb source masses. Each cylinder had a mass of 12.75 kg. The total mass of the 24 cylinders was 306.0 kg.
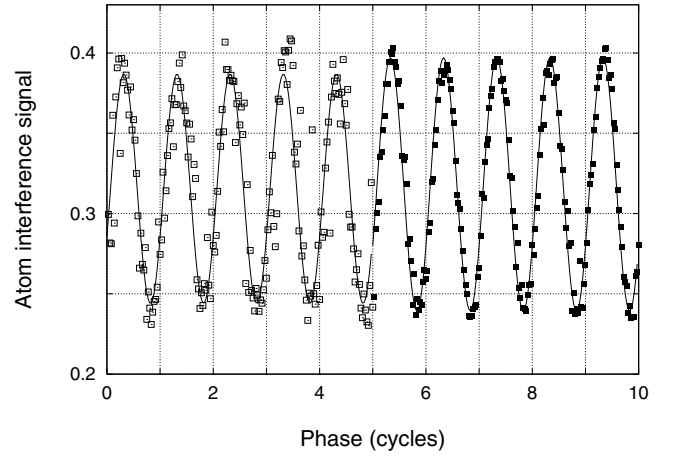
4 Atom interferometer operation and characterization

In the gravimeter configuration, the atom interferometer operating with a single sample of atoms launched in the fountain, the main phase term is the one induced by Earth's gravity

$$\phi(g) = k_{\text{eff}} \, g \, T^2 \qquad (4)$$

where $\hbar k_{\text{eff}}$ is the momentum transferred to the atoms by a Raman pulse. The observed interference signal is shown in Figure 5. The fraction of atoms in the $F = 2$ state is plotted as a function of the phase ϕ_{L}, which is electronically added to the Raman lasers before the final $\pi/2$ pulse. The total phase is in this case the sum of $\phi(g)$ and ϕ_{L}. Each data point results from a single launch of an atomic cloud 80 cm above the center of the MOT and requires 5.5 s. The phase step is $10°$. The phase change due to the varying Doppler effect during the atoms flight was cancelled by chirping the lasers' frequency.

The upper mirror was mounted on a vibration isolation system (HWL Scientific Instruments AVI 350–M(L)). The optical table holding the apparatus is placed on air legs with active position stabilization (Newport RS 2000). We compared interferometer signals with mirror isolation platform off and on, as shown in Figure 5. The signal-to-noise ratio, defined as the ratio between twice the fringe amplitude and the rms noise, is 7 in the first case and 18 in the second case. In the latter, remaining noise is mainly amplitude noise related with fluctuations of the Raman beams intensities. The pulse spacing T can be increased

up to 150 ms, but the phase noise induced by mirror vibrations drastically reduces the fringe visibility. A gravity gradient measurement is obtained by two vertically separated acceleration measurements. The simultaneous realization of these measurements overcomes the stringent limit set by phase noise thanks to common-mode noise rejection. The Raman sequence interval T, as well as the gradiometer sensitivity, can then be increased up to the limit set by experimental constraints. If g_{low} and g_{up} are the gravity acceleration values at the position of the lower and upper interferometers, the differential phase shift is

$$\phi(\Delta g) = k_{\text{eff}} \, (g_{\text{low}} - g_{\text{up}}) \, T^2. \qquad (5)$$

As discussed above, the gradiometer requires two clouds of cold atoms moving with the same velocity at the same time, but vertically displaced. A vertical separation of 35 cm for atoms launched 60 cm and 95 cm above the MOT requires a launch delay between the two clouds of about 100 ms. In the present apparatus, the two atomic clouds are prepared using the juggling technique. In the final configuration, a 2D-MOT will be used for faster loading of the MOT [19].

The Earth's gravity gradient ($\sim 3 \times 10^{-6}$ s^{-2}) corresponds to a relative phase shift that, for a vertical distance Δz of 35 cm and a time interval $T = 100$ ms between the Raman pulses, is expected to be 175 mrad. A sensitive measurement of the relative phase of the two interferometers is obtained by using an ellipse fitting method [22] to cancel common–mode phase–noise. The interference signal of the upper interferometer is plotted versus that of the lower (Fig. 6). The data then describe an ellipse and the relative phase shift can be obtained from its eccentricity and rotation angle. For an integration time of 900 s, the typical rms noise of the experimental data with respect to

Highlight Paper
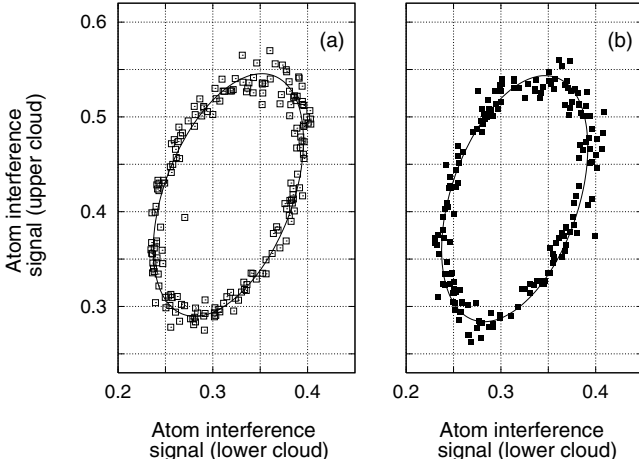
Fig. 6. Signal from the gradiometer with $T = 20$ ms. The fringes from the upper gravimeter are plotted versus the fringes from the lower interferometer. The relative phase can be extracted from the elliptic fit parameters. The mirror isolation system was on in (a), off in (b). The error on the relative phase is ~10 mrad in both cases.

Fig. 7. Phase shift induced by applying a magnetic field pulse with different amplitudes to the lower interferometer for $T = 100$ ms delay between Raman pulses.

the fitting ellipse is 0.005; as a consequence, the phase shift can be determined with an uncertainty of about 100/1, limited by amplitude noise, and uncorrelated phase noise.

To adjust the operating point of the gradiometer, a controlled phase shift was added to the lower interferometer using a magnetic field pulse, acting on the $m_F = 0$ atoms via the second–order Zeeman effect. The resulting phase shift can be written as

$$\Delta\phi_B = 2\pi \, \nu_{z,\mathrm{II}} \left(B^2\right) \int_0^{t_m} \left(B^2_{\mathrm{low}}(t) - B^2_{\mathrm{up}}(t)\right) \mathrm{d}t \quad (6)$$

where $\nu_{z,\mathrm{II}}(B^2) = 57.515$ GHz/T^2 is the second order Zeeman shift coefficient for ^{87}Rb, t_m is the duration of the magnetic pulse, B_{low} and B_{up} the magnetic field values at the lower and upper accelerometer, respectively.

In this case, a knowledge of the pulsed magnetic field is needed for a precise gradient measurement, although it is not critical in the double–differential scheme for the G measurement where only stability matters. The magnetic field in the interferometric region was mapped for different current values in the bias coils using atoms in different m_F sublevels as probes. A sample of cold atoms in the $F = 2$ state was repeatedly launched in the interferometer tube and a selected velocity class was transferred to the $F = 1$ state with a Raman pulse before reaching the inversion point. The atomic sample was then transferred back to the $F = 2$ state with a π Raman pulse and selectively detected. The delay of the second pulse was varied, in order to interact with the free–falling atoms at different vertical positions. This measurements also provide the optimal value for the Raman beams frequency ramp, which is 25.1354(3) MHz/s corresponding to a gravity acceleration g of 9.8056(1) m/s^2. In Figure 7 a direct measurement of the magnetically–induced phase shift is shown. Each point results from an elliptic fit on a set of gradiometric measurements for a certain current value in a bias coil. The
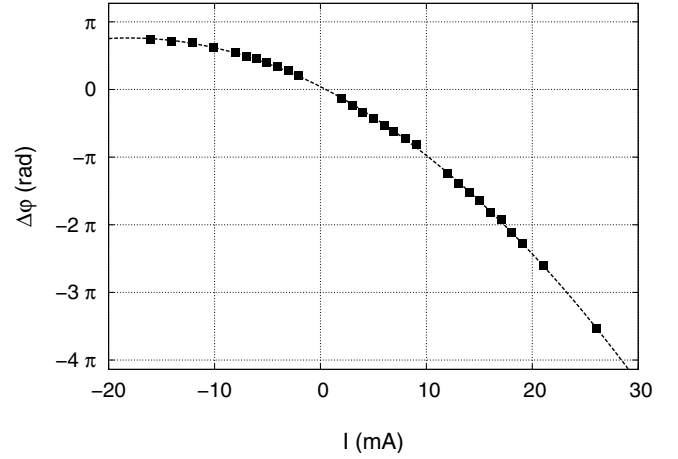
parabolic fit does not cross the axis origin but is shifted by 125 mrad. This vertical offset should be induced by the Earth's gradient that is constantly present during the whole set of measurements. This result differs from the value of 175 mrad produced by the Earth's gravity gradient. The difference can be attributed to the Coriolis effect.

For an atomic velocity component $\mathbf{v}_{EW}$ along East-West direction, the phase induced by the Coriolis effect is

$$\Delta\phi_C = 2 \, \mathbf{\Omega} \cdot (\mathbf{v}_{\mathrm{EW}} \times \mathbf{k}_{\mathrm{eff}})T^2 \quad (7)$$

where $\mathbf{\Omega}$ is the Earth's rotation frequency ($\mathbf{\Omega} = 7.29 \times 10^{-5}$ rad/s). At the lab location (latitude $\theta_{lat} = 43°47'$), a $\mathbf{v}_{EW}$ component of 1 cm/s introduces a $\Delta\phi_C$ corresponding to an acceleration $\Delta a = 2 \, \mathbf{\Omega}\mathbf{v}_{\mathrm{EW}} \cos\theta_{lat} = 10^{-7}g$. In the same conditions, the resulting signal for the gradiometer configuration is proportional to the horizontal velocity difference between the two atomic samples:

$$\Delta\phi_C = 2\mathbf{\Omega} \cdot (\mathbf{\Delta v}_{\mathrm{EW}} \times \mathbf{k}_{\mathrm{eff}})T^2. \quad (8)$$

The adopted apogees, placed at 60 and 95 cm above the MOT, require a launch velocity difference for the two clouds of about 0.8 m/s. This implies a horizontal velocity difference of 0.8 mm/s/mrad of vertical misalignment. The resulting phase difference corresponds to $8 \times 10^{-9}g$/rad. This effect can be minimized by a velocity selection of the atoms launched in the interferometer [23] and by stabilizing the vertical direction of the fountain. However, for the determination of G, the signal is detected as a function of the source masses positions so that constant rotational contributions cancel.

5 Detection of source masses and measurement of G

In order to test the apparatus and to show the possibility of detecting the effect of external source masses, the
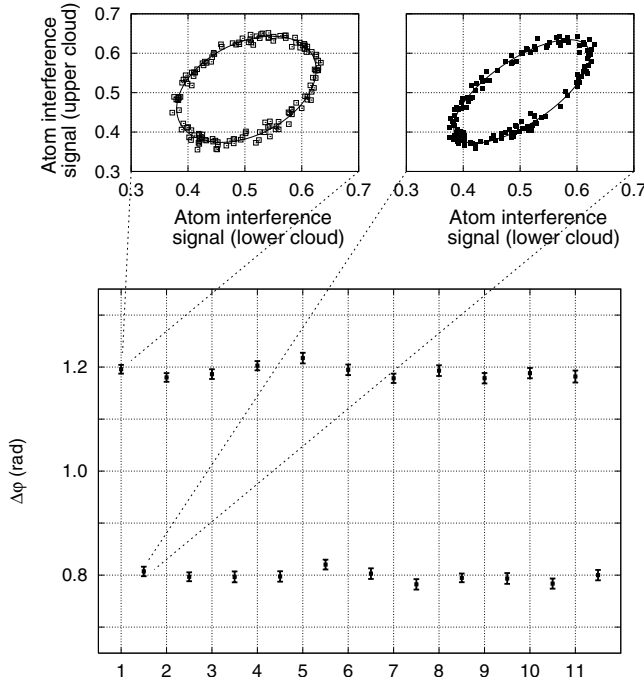
Fig. 8. Gravitational phase shift detected for the two positions of the source masses. The experiment was performed with Pb masses and data were analyzed using the ellipse fitting method. Each data point results from a fit over 144 sequences with a phase step of 5° for the local oscillator. The acquisition time for each point is 15 minutes. The translation of the source masses between two consecutive measurements required ∼100 s. The full data set for two measurements in different configurations are also shown in the upper part of the figure.

interferometer was operated in gradiometer configuration and a set of Pb masses was used.

Pb cylinders had the shape and arrangement as described in Section 3.5. Masses were alternately set in the positions corresponding to the configuration (1) and the configuration (2) shown in Figure 1. In the first case, the acceleration induced on the atoms in the upper cloud is in the –z-direction and the acceleration for the lower cloud is in the +z-direction. The sign of the induced acceleration is changed, moving the masses to the configuration (2) with respect to the atomic clouds. By evaluating the difference between consecutive measurements, a reduction of systematic effects, due for instance to spatially inhomogeneous spurious accelerations, Earth's gravity gradient, inhomogeneous electric and magnetic fields and inertial forces, is achieved.

In Figure 8, the differential phase shifts measured for Pb source masses in the two configurations are reported. The pulse spacing between the Raman pulses has been set to $T = 150$ ms. The total data acquisition time was about 7 hours. Each phase shift measurement in one masses configuration was compared with the mean value between the previous and the following measurement in the other masses configuration to take into account long term drifts. Considering the differences of the obtained couples of values, the resulting phase shift from the whole data set
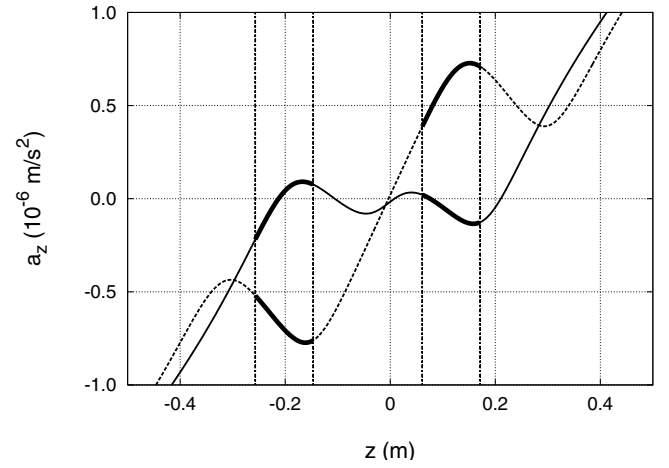
Fig. 9. Vertical acceleration computed for the final experiment with tungsten source masses in two positions. The Earth's gravity gradient was considered. The solid line corresponds to configuration (1) and the dashed line to configuration (2). The spatial regions corresponding to the atomic trajectories for the two interferometers are highlighted.

is 393(4) mrad. Numerically integrating the gravitational signal of the two sets of masses and their holding platforms, we obtain $G = 6.64(6) \times 10^{-11}$ m^{3}kg^{-1}s^{-2}.

To reach the planned accuracy of $\Delta G/G = 10^{-4}$ in the measurement of G, an optimization and characterization of the interferometer and source mass apparatus are required.

The source masses material for the final G measurement is a sintered alloy made of tungsten (95.3%), nickel (3.2%) and copper (1.5%) (Plansee INERMET IT180). This material is non–magnetic and has a typical density of (18000 ± 200) kg/m^3. The 24 cylinders for the experiment come out of the same furnace run. Then the cylinders undergo a hot isostatic pressing (HIP) treatment at $T = 1200$ °C, $P = 1000$ bar which improves the homogeneity of the material. Characterization tests on this material were performed before and after the HIP treatment. Samples were observed with a microscope to detect internal holes; holes, with a typical diameter of ∼150 μm, were reduced to a negligible size by the HIP treatment. The material mean density was measured through a double weighting (in air and in water) at constant temperature. An ultrasonic test was performed to study its homogeneity that also showed a significant improvement after the HIP procedure. We measured the dimensions and deviations from the cylindric shape and verified that they can be machined with a precision of 1–2 μm. A sample cylinder was cut into blocks of $(25 \times 25 \times 44)$ mm^3 to characterize the internal density distribution. The results of all tests show that masses should not affect the final accuracy planned for the G measurement.

The parameters of the atom interferometer must be optimized considering the shape of the gravitational field produced by the source masses. For the configuration (1) in Figure 9, selected atomic trajectories will maximize the phase difference between the two interferometers. Keeping

Highlight Paper

the same atomic trajectories, the source masses will be moved to configuration (2) in which the phase difference term has minimum sensitivity to the atomic position. In this way, the interferometers will be realized where the acceleration is stationary for both configurations. $\Delta G/G = 10^{-4}$ can be reached assuming for the atoms an uncertainty of 1 mm for the position and 5 mm/s for the velocity. Such precision levels on atomic motion knowledge has already been achieved and measured by time–of–flight techniques. Higher levels of precision and accuracy are imposed on the knowledge of the distance between the source masses (10 μm) and of the relative positioning (100 μm). This will be achieved with a combination of precise mechanical positioning by means of stable translational mounts and direct optical measurement of the cylinders position during the experiment.

6 Conclusions

The apparatus developed to measure G using a new scheme based on atom interferometry was presented. The atom interferometer is used to measure the gravitational field produced by source masses. A differential scheme, realized by an atom juggling procedure, was implemented working as a gravity-gradiometer, thus reducing common-mode noise. The result of a preliminary experiment was reported in which, using Pb source masses, G was measured with a relative uncertainty of 1%. Further improvements in the Rb atomic fountain, a reduction of noise sources, and the use of well characterized W source masses will allow to reach the projected accuracy of 1 part in 10^4 in the measurement of G.

References

1. *Atom interferometry*, edited by P.R. Berman (Academic press, 1997)
2. A. Miffre, M. Jacquey, M. Büchner, G. Trénec, J. Vigué, Phys. Scripta **74**, C15 (2006)
3. A. Peters, K.Y. Chung, S. Chu, Nature **400**, 849 (1999)
4. M.J. Snadden, J.M. McGuirk, P. Bouyer, K.G. Haritos, M.A. Kasevich, Phys. Rev. Lett. **81**, 971 (1998)
5. S. Fray, C.A. Diez, T.W. Hänsch, M. Weitz, Phys. Rev. Lett. **93**, 240404 (2004)
6. G.M. Tino, "High precision gravity measurements by atom interferometry", In *A Relativistic Spacetime Odyssey - Proceedings of JH Workshop*, Firenze, 2001 (World Scientific, 2003); also, G.M. Tino, Nucl. Phys. B (Proc. Suppl.) **113**, 289 (2002)
7. S. Dimopoulos, A.A. Geraci, Phys. Rev. D **68**, 124021 (2003)
8. G. Ferrari, N. Poli, F. Sorrentino, G.M. Tino, Phys. Rev. Lett. **97**, 060402 (2006)
9. J.M. McGuirk, G.T. Foster, J.B. Fixler, M.J. Snadden, M.A. Kasevich, Phys. Rev. A **65**, 033608 (2002)
10. T.L. Gustavson, P. Bouyer, M.A. Kasevich, Phys. Rev. Lett. **78**, 2046 (1997)
11. F. Yver-Leduc, P. Cheinet, J. Fils, A. Clairon, N. Dimarcq, D. Holleville, P. Bouyer, A. Landragin, J. Opt. B: Quant. Semiclass. Opt. **5**, S136 (2003)
12. *HYPER, Hyper Precision Cold Atom Interferometry in Space, Assessment study report, ESA-SCI (2000) 10*
13. C. Bordé, G.M. Tino, F. Vetrano, 2004 Aspen Winter College on Gravitational Waves (Available online at: `http://www.ligo.caltech.edu/LIGO_web/Aspen2004/pdf/vetrano.pdf`, to be published)
14. R.Y. Chiao, A.D. Speliotopoulos, J. Mod. Opt. **51**, 861 (2004)
15. A. Roura, D.R. Brill, B.L. Hu, C.W. Misner, W.D. Phillips, Phys. Rev. D **73**, 084018/1 (2006)
16. M. Fattori, G. Lamporesi, T. Petelski, J. Stuhler, G.M. Tino, Phys. Lett. A **318**, 184 (2003)
17. P.J. Mohr, B.N. Taylor, Rev. Mod. Phys. **77**, 42 (2005)
18. M. Kasevich, S. Chu, Appl. Phys. B **54**, 321 (1992)
19. T. Petelski, *Atom interferometers for precision gravity measurements*, Ph.D. thesis, Università di Firenze (2005); available online at `www.fi.infn.it/sezione/esperimenti/MAGIA/home.html`
20. R. Legere, K. Gibble, Phys. Rev. Lett. **81**, 5780 (1998)
21. L. Cacciapuoti, M. de Angelis, M. Fattori, G. Lamporesi, T. Petelski, M. Prevedelli, J. Stuhler, G.M. Tino, Rev. Sci. Instrum. **76**, 053111 (2005)
22. G.T. Foster, J.B. Fixler, J.M. McGuirk, M.A. Kasevich, Opt. Lett. **27**, 951 (2002)
23. A. Peters, K.Y. Chung, S. Chu, Metrologia **38**, 25 (2001)
24. P. Cheinet, B. Canuel, F.P.D. Santos, A. Gauguet, F. Leduc, A. Landragin, `arXiv:physics/0510197`

Highlight Paper